On the Feasibility of EEG-based Motor Intention Detection for Real-Time Robot Assistive Control

Ho Jin Choi[1†*], Satyajeet Das[1†], Shaoting Peng[1†], Ruzena Bajcsy[1] and Nadia Figueroa[1]

***Abstract*— This paper investigates the feasibility of using EEG-based intention detection for real-time robot assistive control, with a focus on motor intention prediction. The proposed approach involves two pipelines: i) an offline pipeline that collects and processes EEG data as well as motion data to train a classifier for motion intention prediction and biological interpretation, and ii) an online pipeline that uses the trained classifier to predict a human's motor intention and couples it with a robot to perform assistive control. We adopt and modify the state-of-the-art EEG sample covariance matrix feature representation by using EEG signal derivatives and tangent space projection as features for an SVM classifier that can run in real-time. With this, Our system excels with the highest accuracy of 86.88% in real-time settings, and it achieves an impressive 70% accuracy in real robot experiments. We show in a real-robot experiment that our online pipeline is able to detect the onset of motion purely from EEG signals and trigger a robot to perform an assistive task.**

I. Introduction

As robots evolve from being mere tools to becoming intelligent collaborators, the importance of comprehending and predicting human intentions has taken center stage in the robotics community. Particularly in scenarios where robots offer essential physical aid to the elderly or individuals with disabilities, the prediction of intentions becomes pivotal in establishing responsive and harmonious interactions that seamlessly blend human needs with robotic assistance [1].

The term "human intention prediction" encompasses a robot's capability to deduce the actions or choices that a human is likely to undertake. This predictive prowess empowers robots to dynamically align their behaviors, responses, and maneuvers in a proactive manner. In this work, our focus is deliberately narrowed down to motor intention prediction, as the overarching term "intention" encompasses a broad spectrum of meanings [2]. Motor intention estimation specifically refers to forecasting a human's velocity, location, or force trajectory within a confined time frame, employing the principles of state estimation. Moreover, this extends to foreseeing the states of objects subsequent to a brief period of human movement. The crux of motor intention prediction lies in the quest for optimal solutions amid multiple potential trajectories. To achieve this, constructing a model of the human sensorimotor system becomes imperative in order to prune the range of potential outcomes. An approach to crafting this sensorimotor model lies in the application of electroencephalography (EEG) to directly decode human cognitive processes [3]. EEG captures electrical signals, a summation of postsynaptic potentials, emitted by numerous pyramidal cells located within the brain cortex, acting as dipoles [4].

The viability of EEG for brain-computer interface (BCI) and brain-machine interfaces (BMI) applications has been repeatedly demonstrated, given its accessibility and minimal invasiveness [5]. Conventionally, BCI/BMI encompasses five stages: i) signal acquisition, ii) preprocessing, iii) feature extraction, iv) classification, and v) control interface [6]. In contrast to external sensors or explicit input mechanisms, EEG measurements can be collected unobtrusively without interfering with the user's actions. This aspect gains importance in scenarios prioritizing naturalness, particularly evident in assistive robotics catering to individuals with motor impairments. Although EEG might not capture signals from deep brain structures like the thalamus, it effectively captures surface information from the frontal lobe and motor cortex, which are intricately connected to the thalamus for signal transmission and reception.

Contributions: In this paper, we present an online pipeline for identifying and utilizing motion-related signals for robot control and offer an in-depth analysis of the collected EEG signals. Our approach has three stages:

1) The identification of time window size, frequency, and classifier through analysis of EEG signals
2) The fitting of a body movement classification model using calibration data for a specific subject
3) The online application of the classification outcomes to robot control for executing assistive actions

Paper Organization: After listing related works in Section II, we describe our methods in Section III. Then, in Section IV we introduce our experiments, followed by showcasing and comparing the results in Section V. Finally, in Section VI the conclusion and future works are discussed.

II. Related works

A. EEG features for classifiers

An accurate way to get the features of brain signals through EEG is to solve the inverse problem of 3D source localization [7], which gives the region and its activation degree. However, this requires a rough model of the human head using MRI scans or a canonical model. Also, computation time is too long to be used in an online manner. Therefore, researchers have sought to identify certain brain patterns now common in literature, particularly the Readiness Potential (RP) and Event-Related Desynchronization/Synchronization (ERD/ERS) [8]. To identify these

† Equal contribution, listed in alphabetical order.

*Corresponding author: cr139139@seas.upenn.edu

[1]All authors are with School of Engineering and Applied Science, University of Pennsylvania, Pennsylvania, PA 19104 USA.

patterns, raw EEG signals or their frequency obtained from a fast Fourier transform (FFT) or wavelet transform (WT) has been used as the EEG feature to train classifiers. Also, time derivatives have been tested and compared with raw EEG signals [9], [10]. EEG signals from multiple channels are known to be spatially related to each other. Therefore, there have been efforts to use spatial filters [10], graph structures [11], or sample covariance matrices [12] to capture the relationship between electrodes.

B. Online motor intention classification using EEG

For human motion tracking and prediction, researchers have conventionally employed EMG-based techniques [13], [14], camera-marker-based methods, or a fusion of the two. These methods excel in detecting precise positional and force-related information pertaining to different body segments. Nevertheless, they do not detect the motor intention from the source, the brain. The utilization of EEG offers a means to acquire rudimentary insights into movement through a phenomenon known as cortical potentials, such as readiness potential (RP) [15], [16]. Debates exist around whether the onset of cortical potentials invariably indicates imminent physical action. However, it is generally observed that potentials occur approximately 500 ms before a voluntary motion starts, with a potential occurrence occurring 200 ms before such a motion is deemed inevitable. There have been efforts to detect RP for robotic control. Nonetheless, the detection of RP typically necessitates the aggregation of EEG signals across multiple trials, posing challenges for real-time single-trial RP detection. Also, well-known noise and artifact issues in EEG make detection harder.

The surge of deep learning techniques has increased the accuracy of brain signal classification. Convolutional neural networks (CNNs) emerged as formidable tools adept at deciphering nonstationary and nonlinear intricacies within EEG data [17]. Also, an intriguing fusion of neuromorphic computing and BCIs emerged, with spiking neural networks (SNNs) occupying a central role [18]. However, they mainly work offline, making them hard to use in online control scenarios. Therefore, for BCI scenarios, simple classifiers such as linear discriminant analysis (LDA) [19], Support Vector Machines (SVMs) [20], [21], fuzzy logic-based classifiers [22], Gaussian [23] and Bayesian [24] classifiers that can deal with uncertainty, and shallow neural networks [25], [26], [27], [28] are more suitable. The fusion of SVMs, Random Forests, and Artificial Neural Networks by Kucukyildiz et al. [29] has been used to elevate the average sensitivity. However, these works are still mostly effective offline.

Racz et al. [30] pioneered online cortical potential classification, attaining a 62.6% binary classification accuracy. The accuracy of online cases decreases compared to offline cases due to the fact that single-trial detection is more difficult and most blind source artifact removal methods are hard to use in an online manner to make the signals cleaner. Our proposed method now establishes the state-of-the-art standard, achieving an impressive 86.88% in real-time settings, and 70% accuracy in real robot experiments.

III. Methods

In this section, the real-time EEG-based intention detection method is explained. We begin by introducing some preliminaries, which are the sample covariance matrix and the SVM classifier. Next, we start introducing the feature extraction part, followed by offline training and online execution pipelines.

A. Preliminaries

1) Sample Covariance Matrix: Given a multivariate signal $X \in \mathbb{R}^{W \times n}$ where n is the number of channels and W is the size of the window, the sample covariance matrix is defined as $C = Cov(X) = \frac{X^T X}{(n-1)}$. If W is sufficiently larger than n, this covariance matrix is a symmetric positive definite (SPD) matrix, which lies on the Riemannian manifold [31]. The mean of N points on the manifold of the SPD matrix, μ, is required as a reference point for tangent space projection, and it is iteratively computed by the expectation-maximization method [32] as

$$u = \frac{1}{N}\sum_{i=1}^{N} \mathrm{Log}_{\mu}(x_i), \quad \mu = \mathrm{Exp}_{\mu}(u) \tag{1}$$

where Log_P stands for Riemannian logarithm mapping for SPD matrix P, projecting a point to the P's tangent space, and Exp_P stands for Riemannian exponential mapping for SPD matrix P, projecting a point on P's tangent space back to the manifold. Both mappings are defined as

$$\begin{aligned} \mathrm{Log}_P(P^*) &= S^* = P^{\frac{1}{2}} log(P^{-\frac{1}{2}} P^* P^{-\frac{1}{2}}) P^{\frac{1}{2}} \\ \mathrm{Exp}_P(S^*) &= P^* = P^{\frac{1}{2}} exp(P^{-\frac{1}{2}} S^* P^{-\frac{1}{2}}) P^{\frac{1}{2}} \end{aligned} \tag{2}$$

where P^* also lies on the SPD matrix manifold and S^* is a point on tangent space, which is a symmetric matrix. To classify biosignals, several works [31] have used the Riemannian manifold to find a mean of data points or covariance matrices, project all data points to the tangent space of the mean, and use the upper triangle of the tangent space points with classic classifiers, $s^* = vec(S^*)$. This tangent space vector can be used as a feature for classification.

2) Classifier: The Radial Basis Function Support Vector Machine (RBF-SVM) is a powerful classification algorithm, particularly effective for non-linearly separable datasets. In an RBF SVM, the decision boundary is determined by a kernel function that maps the data into a higher-dimensional space, where it can be linearly separated. The RBF kernel function is defined as:

$$K(s, s_i) = \exp(-\gamma \cdot ||s - s_i||^2) \tag{3}$$

The kernel function measures the similarity between data point s and support vector s_i, where γ controls the shape of the decision boundary. The SVM classifier is defined as:

$$y = \mathrm{sign}\left(\sum_{i=1}^{M} (\alpha_i \cdot y_i \cdot K(s, s_i)) + b\right) \tag{4}$$

In this equation, y represents the predicted label, M is the number of support vectors, α_i are Lagrange multipliers,

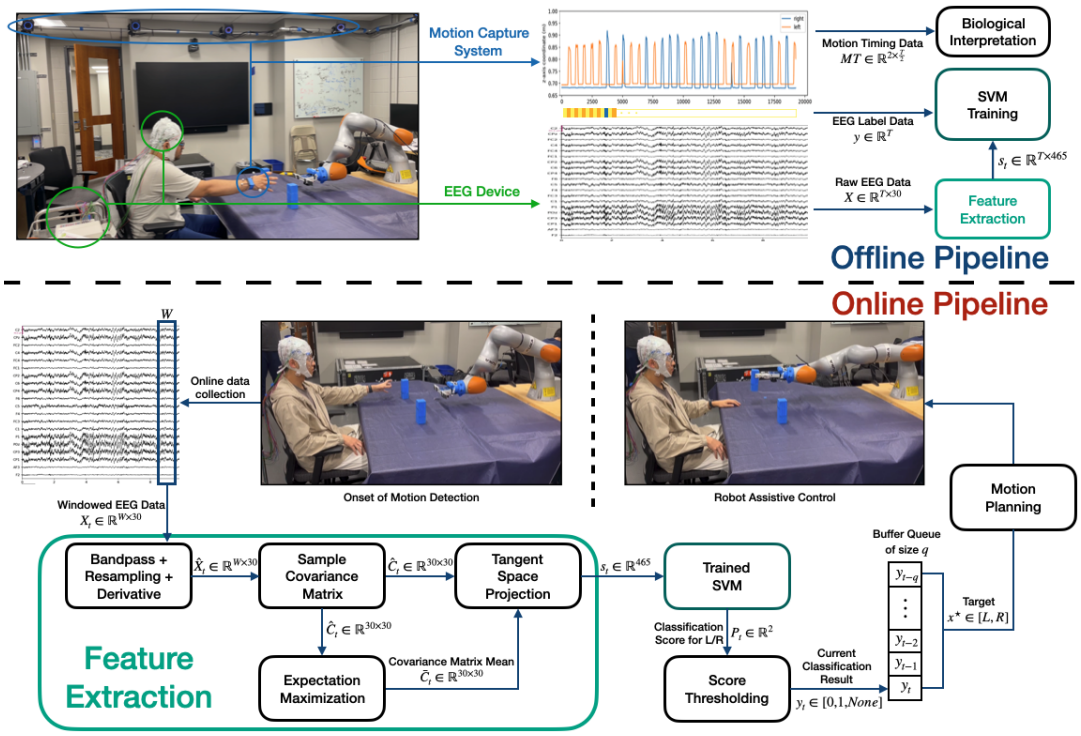

Fig. 1: Our offline and online pipeline: The upper part is the offline pipeline, which first gathers the raw EEG data and the corresponding labels, as well as the motion data given by the motion capture system. Then the same feature extraction part is done, and the output features with labels are used to train the classifier. The motion data is used further for biological interpretation. The lower part is the online pipeline, which starts from the EEG data stream and extracts the tangent space projected covariance matrix as features for the classification. Some post-processing follows to ensure the rightness of the classification results. Finally, the robot moves to the classified object and hands it over to the human.

y_i are class labels, $K(s, s_i)$ is the RBF kernel, and b is the bias term. This equation computes a weighted sum of kernel values between input s and support vectors s_i using learned weights (α_i) to make binary classifications, effectively mapping features like EEG data to labels.

B. Pipeline

In this section, we will introduce how we get predictions $y \in [left, right]$ from raw EEG signals $X \in \mathbb{R}^{W\times 30}$. Then, in the experiments section, we close the loop by introducing how EEG signals X are obtained, and how y is used to control the robot arm.

1) EEG Feature Extraction: Let us denote a sequence of raw EEG data consisting of 30 channels, which commences at time point t and spans a duration of T, as $X_t \in \mathbb{R}^{W\times 30}$. In order to ensure optimal compatibility with both our classifier and robot control, we resample the data from its original sampling rate of 250 Hz to a new rate of 160 Hz.

It is important to note that the amplitude of EEG data exhibits considerable variability across different subjects and even within multiple trials of the same subject. To address this inherent inconsistency in EEG data, we propose a data processing technique involving signal differentiation, represented as $\hat{X}_t = X_t - X_{t-1}$. This approach not only preserves the tendency of the data that are pertinent to capturing valuable brain signals such as the readiness potential (RP) and event-related desynchronization/synchronization (ERD/ERS), but also mitigates undesired disparities between trials, thus enhancing the generalizability of our findings. A comparative analysis between our derivative method and non-derivative approach is presented in Section V.

Following the aforementioned preprocessing procedures, we employ the sample covariance matrix method, which has been introduced in Section III-A, to derive the feature denoted as $s_t \in \mathbb{R}^{465}$ where 465 corresponds to the flattened upper triangle of the tangent space covariance matrix denoted as $C \in \mathbb{R}^{30\times 30}$. It is noteworthy that this particular feature is utilized consistently across all methodologies presented in this paper; thus, any reference to "feature extraction" in the subsequent discussions pertains to it.

2) Offline Data Collection Pipeline: In this pipeline, we align EEG data with OptiTrack data at a frequency of 160 Hz to generate our data both for training and interpretation. As shown in Figure 1, our dataset consists of following parts:

$$DS = \{X, y, MT\} \tag{5}$$

The raw EEG signal X_{raw} has the shape $(T, 30)$. For the online usage, we apply a time window of size W with step size 1 to segment it and concatenate the windows together, resulting in an overlapped windowed data $X \in \mathbb{R}^{T\times W\times 30}$, $y \in \mathbb{R}^{T}$ is the corresponding label of 'left' and 'right' for every time step (separated by the auditory cues in our experiments), and $T_{motion} \in \mathbb{R}^{2\times N}$ denotes the onset of motion time for left and right grasping given by the motion

capture system (N times each).

Once the dataset has been established, the raw EEG data X undergoes the feature extraction stage, resulting in the features represented as $s \in (T_{L/R}, 465)$. Subsequently, these extracted features, along with the corresponding labels y, are utilized to train our Support Vector Machine (SVM) classifier. For the evaluation phase, a testing dataset is constructed using a similar procedure. Timing information is collected by combining the motion time T_{motion} with the cue time y. This fusion of data allows us to assess both intention detection and motion detection accurately.

3) Online Motion Prediction Pipeline: As for the online pipeline, we are using the EEG data stream for consistent SVM classification, so the data size is different from the training phase. We apply a window of size W and step size s to achieve real-time performance. At every time step, current windowed data $X_t \in \mathbb{R}^{W\times 30}$ is collected and goes over the feature extraction part to get the corresponding feature $S_t \in \mathbb{R}^{465}$. Unlike most offline classification papers, we proposed two new methods that are used to boost the performance of real-time robot assistive control.

Regarding the online pipeline, our approach involves the utilization of the EEG data stream for continuous real-time SVM classification. In this phase, the data size varies compared to the training phase. We implement a sliding window approach with a window size of W and a step size of s to facilitate real-time processing. At each time step, the current windowed EEG data $X_t \in \mathbb{R}^{W\times 30}$ is collected and passed to the feature extraction process, yielding the corresponding feature vector $s_t \in \mathbb{R}^{465}$ for the classification.

Notably, for real-time robot assistive control, it is imperative to recognize that a direct application of the same pipeline employed in offline classification may not be suitable. This is primarily because the offline classification can potentially yield erratic predictions at some time steps that are unsuitable for the smooth and efficient control of the robot, although the total classification accuracy can be high. To deal with it, in contrast to the majority of offline classification studies, our work introduces two novel methods designed to enhance the performance of real-time robot assistive control.

Score Thresholding: During the prediction phase, our approach does not directly provide the output class but rather yields a classification score denoted as $P_t \in \mathbb{R}^2$ for the left and right classes. These scores are constrained such that they sum to 1, effectively behaving like probabilities for each class. The final prediction is made only if one of these class probabilities surpasses a predefined threshold denoted as δ. This strategy serves to mitigate the adverse impact of noisy EEG data on the classification outcome.

Buffer Queuing: Despite the incorporation of score thresholding, the performance of robot control can still be occasionally influenced negatively. For instance, in situations where there are 70 correct predictions and 30 incorrect ones, the timing may inadvertently lead to one of the incorrect results being selected for robot control. To enhance the precision of robot control further, we implement a buffer queue denoted as $\mathcal{BQ}$ with a capacity of q. This queue is designed to store the most recent q thresholded classification results and is updated at each time step. When it comes to the time for the robot to execute a movement, the element that occurs most frequently in the queue is selected as the target denoted as $x^\star$ for the robot's motion planning.

Motion Planning Once the target for the robot's end-effector x^* is detected, we feed this to a linear controller $\dot{x} = A(x - x^*)$ that will drive the robot to the desired target. Then, if the error is within the threshold, the robot will grasp the object and move to a defined hand-over position.

IV. Experiments

A. Robot experiment setup

We use a Bittium Neurone wet EEG device to get a stream of brain signals at 250 Hz using the International 10–20 system with 30 electrodes, a KUKA iiwa 7 robot, and an Optitrack motion tracking system at 100 Hz to check the onset of motion time for the subject. Because of the individuality of subjects and the fact that subjects' states change over time, we fit the classifier using a few samples from the subject in the offline pipeline before doing the robot control. During the offline data collection stage, the subject is given auditory cues for left or right hand grasping, which last for 2 seconds. Then, the subject rests for 2 seconds and repeats that. After 30 random trials of left and right grasping, we go to online practice, where our robot experiment setup assumes a robot and a human mirroring each other in a shared workspace with two objects in front of the human, as in Figure 1. The subject is given an auditory cue that tells the subject to move, and the subject moves randomly to the left or right. The robot, based on the human's movement to the left or right grasping, moves in that direction based on the classification result and gives the object in that direction to the human, which is not reachable by the human.

B. Classifiers, Features, and Hyperparameters Selection

Based on our pipeline, we first conduct an evaluation of diverse hyperparameters. These encompass pivotal parameters such as the window size W employed in online data processing and the selection of distinct frequency bands for signal filtering. This comprehensive analysis serves the primary objective of elucidating the intrinsic relationship between different brain frequency bands and motor movements. Subsequently, based on the optimal hyperparameters, we proceed to assess the combination of different features with or without the derivative method, including the raw signal, conversion to covariance matrix, and projection to tangent space. At last, we evaluate the accuracies of different classifiers, including logistic regression, random forest, multi-layer perceptron, and support vector machine. Results of these assessments can be found in Table I, II and III.

C. Motor Movement Dataset Data Processing

We compare the Physio motor movement dataset [33] and our dataset and check the difference between them. The motor movement dataset encompasses 109 participants (42 males, 59 females, 8 N/A) employing 64-channel EEG devices at a sampling frequency of 160 Hz and having diverse

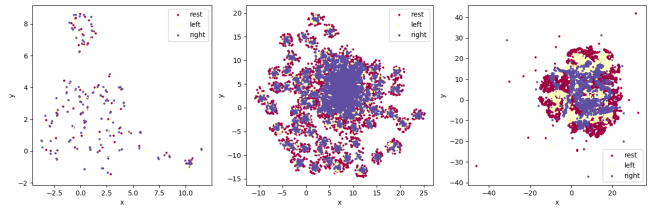

Fig. 2: UMAP results of the Motor Movement Dataset for 109 subjects. The left graph shows the mean of 'rest', 'left', and 'right' for all subjects, and the center graph shows each individual sample of them. The right graph shows UMAP results for a single person.

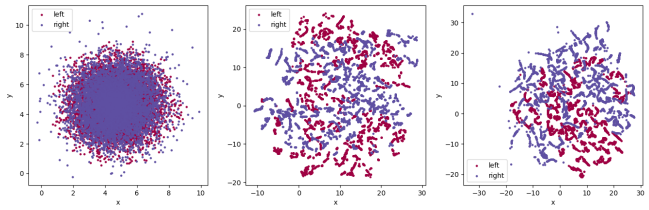

Fig. 3: UMAP results of our dataset on raw windowed data, the upper triangle of the covariance matrix, and tangent space vector.

experimental scenarios, including opening and closing the left or right fist and opening and closing both fists or feet. Each data instance is categorized as either resting or the corresponding motor activity concerning the visual cue. We use runs for three classes from the dataset: 'resting', 'left fist', and 'right fist'. Then, we slice the data between 0.5 and 1.5 seconds after the onset of the cue, which we assume to be near the subject's onset of motion time. For our dataset, the subjects do 15 trials of left and right grasping with the cue and 15 trials of random direction grasping. Using the tracking data, we check the onset of motion timing and slice the data 0.5 seconds before and after the onsets.

V. Results

A. Feature extraction and reduction

To see if the tangent space method extracts meaningful features, we do the dimension reduction of the feature and visualize the reduced dimension feature using Uniform Manifold Approximation and Projection (UMAP) [34] on the motor movement dataset [33] and our dataset. UMAP is similar to t-SNE, which is used for visualizing high-dimensional vectors in 2D or 3D, but it is faster and considers global relationships such as density better than t-SNE.

When we take the mean covariance of each person's action to project all covariance into the tangent space, we can see that actions for different subjects have different features, as shown on the left in Figure 2. Also, if we do feature reduction using individual time-windowed samples, mimicking the online method, we get noisier results. However, if we look at a single person's result, it becomes more distinguishable than considering all subjects. Therefore, this tells us that classification has to be done in an individual manner to get stable results, which can be used for robot control. From our data, we can see that the covariance matrix and tangent space vector have features that are more distinguishable than raw data, as shown in Figure 3.

B. Hyperparameters selection

In this section, we conducted an evaluation of classification accuracies, with a particular focus on two hyperparameters: time window and frequency range. Our chosen model for this evaluation was the RBF SVM, and the results are presented in Table I. Our findings indicate that utilizing a frequency range of 5-15 Hz yielded the most favorable results, which we presume to be due to the presence of RP occurring within the 8-13 Hz range[35]. We observed promising results when extending the time window to 0.5 and 1 second within the 30-40 Hz gamma range, which aligns with its known association with advanced cognitive functions. However, it's important to note that, in our overall analysis, the 5-15 Hz frequency range consistently provided the best performance. Our findings emphasize that achieving the best results hinges on selecting suitable hyperparameters. In our case, the optimal choice was the 5-15 Hz frequency range combined with a 2-second time window, resulting in an impressive accuracy of 86.88%. This highlights the importance of fine-tuning hyperparameters to optimize EEG signal analysis.

C. Feature and model selection

In this section, we conduct a comparative analysis of classification accuracies using various classifiers, including logistic regression, support vector machine (SVM), and multi-layer perceptron (MLP), in conjunction with different feature sets. These feature sets encompass the raw signal data of windowed 30-electrode signals, the upper triangle of the covariance matrix, and the tangent space method, all with and without derivative processing. The detailed results can be found in Table II and Table III.

Examining the feature selection outcomes presented in Table II, it becomes evident that incorporating the derivative processing significantly enhances overall accuracy due to its ability to mitigate disparities between trails, yielding a notable increase of 28.96 percentage points, resulting in an accuracy of 69.10%. When considering feature types, the tangent space projection method emerges as the most effective, achieving the highest accuracy at 86.88%. Regarding the selection of classifiers, as depicted in Table III, we compute the average of the top 3 accuracies from all 6 feature combinations (as shown in Table II) for each classifier to gauge their overall performance. We also conduct the grid search for SVM and MLP, the best result for each is given by regularization parameter $C = 0.1$ and kernel coefficient $\gamma = 0.5$ for SVM, and hidden layer size $(100, 3)$ for MLP. These results indicate that SVM outperforms the other classifiers with an average accuracy of 69.1%.

D. Biological Interpretation

By aggregating the mean probability (classification score) generated by the SVM for left and right motions across each trial and aligning it with the motion timing data obtained from the motion capture system, we construct the left portion

		Frequency Range (Hz)								
		0 - 5	**0 - 10**	**5 - 15**	**10 - 20**	**15 - 25**	**20 - 30**	**25 - 35**	**30 - 40**	**35 - 45**
Time Window (s)	**0.03**	32.47	43.82	**61.80**	33.61	16.54	38.18	31.86	19.92	6.75
	0.06	44.76	41.65	**58.40**	26.56	15.34	28.76	18.36	15.92	37.41
	0.12	12.24	29.53	**69.80**	43.34	22.60	10.47	4.44	9.62	19.34
	0.25	42.99	45.92	**63.82**	32.91	6.25	9.40	15.11	34.25	12.57
	0.5	15.49	33.22	58.705	7.27	8.63	27.42	34.79	**61.51**	6.51
	1	34.01	39.33	57.91	10.37	28.69	48.15	60.17	**80.11**	71.27
	2	11.36	39.03	**86.88**	85.13	79.19	73.02	60.29	42.51	39.43

TABLE I: Accuracies of SVM with various frequency ranges and time windows

	Without derivative			derivative		
Feature	Raw	Covariance	Tangent space	Raw	Covariance	Tangent space
Accuracy (%)	32.84	47.27	40.32	64.15	56.26	**86.88**

TABLE II: Accuracies of SVM with various features

	Accuracy (%)
Linear Regressor	63.12
Support Vector Machine	**69.10**
Multi-Layer Perceptron	45.93
Random Forest	47.47

TABLE III: Averages of the top 3 features accuracies (as shown in Table II) of different models

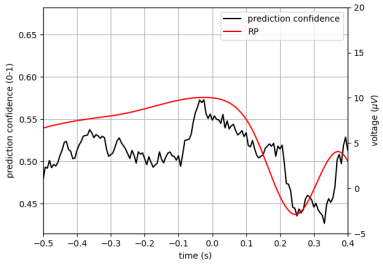

Fig. 4: Mean probability confidence for all left and right trials in black line with respect to the onset of motion and the readiness potential (RP) in red line with the unit of μV reproduced from data provided by Wen et al. [36].

of Figure 4. The point labeled '0s' represents the onset of motion. In this representation, we observe a notable increase in signal intensity from approximately -0.1s to 0s, followed by a subsequent decrease from 0s to 0.3s. These observations can suggest the presence of the readiness potential (RP), as illustrated in the right portion of the figure.

However, while we detect RP-like behavior, it's difficult to detect and disambiguate the onset of motion in a real-time setting given the current technology and state-of-the-art approaches that we have. This arises for two main reasons: the RP signal is very brief, and EEG also detects motion artifacts. We believe that we are detecting a combination of RP and motion-related brain signals at 5-15 Hz. This combined signal can hold potential for robot control as it encapsulates both preparatory brain activity and the intention to execute a specific motion.

E. Real robot results

The accuracy between the two different subjects differed (subject 1: 79.1%, subject 2: 70.8%) but was above 70% as shown in Figure 5 for 24 trials with random movement from the subject. Since the signal related to the left and right movements happened around the onset of motion, which is

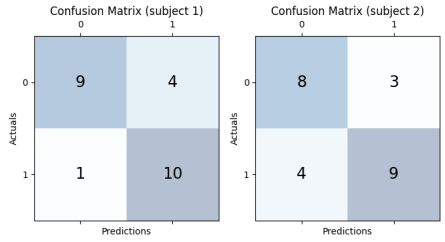

Fig. 5: Confusion matrix of robot experiments for two subjects.

unpredictable, using a queue increased the accuracy of the classification results.

VI. Conclusion and Future Work

In this study, we present two pipelines designed to facilitate EEG-based real-time robot control. The online pipeline is first focused on the extraction of features from raw EEG data for classification. To tackle the noisy signal issue, we then introduce classification score thresholding and buffer queuing methods, which enhance signal stability, enabling control of the robot arm in real-time. The offline pipeline is responsible for the collection and processing of EEG data used for training our classifier. Additionally, this pipeline handles the acquisition of motion data, which is later analyzed for biological interpretation.

Our experimental results demonstrate the effectiveness of the tangent space covariance matrix projection method in extracting robust features that are compatible with multiple classifiers. Among these classifiers, the support vector machine (SVM) exhibits the highest performance. Furthermore, we conduct a comprehensive evaluation of various parameters, including time window size, frequency bands, EEG data features, and classifiers. This analysis allows us to identify the most effective combination for online classification. Leveraging the motion capture system, we investigate the temporal relationship between motion and classification, shedding light on the influence of readiness potential and motor brain signals on the classification outcomes.

In the future, our research direction involves the integration of additional modalities, such as electromyography (EMG), with the aim of improving the quality of neural data. This enhancement may enable us to utilize stable intention signals for robot control even before the commencement of physical movements. Furthermore, we aspire to expand our classification repertoire beyond left and right grasping data, incorporating more complex movements involving the arms or legs, thereby broadening the scope of assistive control.

REFERENCES

[1] A. Sciutti, M. Mara, V. Tagliasco, and G. Sandini, "Humanizing human-robot interaction: On the importance of mutual understanding," *IEEE Technology and Society Magazine*, vol. 37, pp. 22–29, 2018. [Online]. Available: https://api.semanticscholar.org/CorpusID:3812272

[2] D. Kulić and E. A. Croft, "Estimating intent for human-robot interaction," *Advanced Robotics*, 2003. [Online]. Available: https://api.semanticscholar.org/CorpusID:1120056

[3] H. M. Lakany and B. A. Conway, "Understanding intention of movement from electroencephalograms," *Expert Systems*, vol. 24, 2007. [Online]. Available: https://api.semanticscholar.org/CorpusID:5936372

[4] T. Kirschstein and R. Köhling, "What is the source of the eeg?" *Clinical EEG and neuroscience*, vol. 40, no. 3, pp. 146–149, 2009.

[5] K. Värbu, M. Naveed, and Y. Muhammad, "Past, present, and future of eeg-based bci applications," *Sensors (Basel, Switzerland)*, vol. 22, 2022. [Online]. Available: https://api.semanticscholar.org/CorpusID:248775078

[6] M. B. Khalid, N. I. Rao, I. Rizwan-i Haque, S. Munir, and F. Tahir, "Towards a brain computer interface using wavelet transform with averaged and time segmented adapted wavelets," in *2009 2nd International Conference on Computer, Control and Communication*, 2009, pp. 1–4.

[7] C. M. Michel and D. Brunet, "Eeg source imaging: A practical review of the analysis steps," *Frontiers in Neurology*, vol. 10, 2019. [Online]. Available: https://api.semanticscholar.org/CorpusID:93003798

[8] Y. Wang, S. Gao, and X. Gao, "Common spatial pattern method for channel selelction in motor imagery based brain-computer interface," in *2005 IEEE Engineering in Medicine and Biology 27th Annual Conference*, 2005, pp. 5392–5395.

[9] D. A. Andreou and R. Poli, "Comparing eeg, its time-derivative and their joint use as features in a bci for 2-d pointer control," *2016 38th Annual International Conference of the IEEE Engineering in Medicine and Biology Society (EMBC)*, pp. 5853–5856, 2016. [Online]. Available: https://api.semanticscholar.org/CorpusID:172677

[10] M. Menceloglu, M. Grabowecky, and S. Suzuki, "Spectral-power associations reflect amplitude modulation and within-frequency interactions on the sub-second timescale and cross-frequency interactions on the seconds timescale," *PLoS ONE*, vol. 15, 2020. [Online]. Available: https://api.semanticscholar.org/CorpusID:214419358

[11] G. Chen, H. S. Helm, K. Lytvynets, W. Yang, and C. E. Priebe, "Mental state classification using multi-graph features," *Frontiers in Human Neuroscience*, vol. 16, 2022. [Online]. Available: https://api.semanticscholar.org/CorpusID:247187688

[12] A. Barachant, S. Bonnet, M. Congedo, and C. Jutten, "Classification of covariance matrices using a riemannian-based kernel for bci applications," *Neurocomputing*, vol. 112, pp. 172–178, 2013. [Online]. Available: https://api.semanticscholar.org/CorpusID:13873072

[13] L. Bi, A. G. Feleke, and C. Guan, "A review on emg-based motor intention prediction of continuous human upper limb motion for human-robot collaboration," *Biomedical Signal Processing and Control*, vol. 51, pp. 113–127, 2019. [Online]. Available: https://www.sciencedirect.com/science/article/pii/S1746809419300473

[14] E. Trigili, L. Grazi, S. Crea, A. Accogli, J. Carpaneto, S. Micera, N. Vitiello, and A. Panarese, "Detection of movement onset using emg signals for upper-limb exoskeletons in reaching tasks," *Journal of neuroengineering and rehabilitation*, vol. 16, pp. 1–16, 2019.

[15] A. Schurger, P. B. Hu, J. Pak, and A. L. Roskies, "What is the readiness potential?" *Trends in Cognitive Sciences*, vol. 25, no. 7, pp. 558–570, 2021. [Online]. Available: https://www.sciencedirect.com/science/article/pii/S1364661321000930

[16] E. Travers, N. Khalighinejad, A. Schurger, and P. Haggard, "Do readiness potentials happen all the time?" *NeuroImage*, vol. 206, p. 116286, 2020. [Online]. Available: https://www.sciencedirect.com/science/article/pii/S1053811919308778

[17] X. Tang, W. Li, X. Li, W. Ma, and X. Dang, "Motor imagery eeg recognition based on conditional optimization empirical mode decomposition and multi-scale convolutional neural network," *Expert Systems with Applications*, vol. 149, p. 113285, 2020.

[18] P. Batres-Mendoza, E. I. Guerra-Hernandez, A. Espinal, E. Pérez-Careta, and H. Rostro-Gonzalez, "Biologically-inspired legged robot locomotion controlled with a bci by means of cognitive monitoring," *IEEE Access*, vol. 9, pp. 35 766–35 777, 2021.

[19] S. Bhattacharyya, A. Konar, and D. Tibarewala, "Motor imagery and error related potential induced position control of a robotic arm," *IEEE/CAA Journal of Automatica Sinica*, vol. 4, no. 4, pp. 639–650, 2017.

[20] J. Choi, K. T. Kim, J. H. Jeong, L. Kim, S. J. Lee, and H. Kim, "Developing a motor imagery-based real-time asynchronous hybrid bci controller for a lower-limb exoskeleton," *Sensors*, vol. 20, no. 24, p. 7309, 2020.

[21] H. Gao, L. Luo, M. Pi, Z. Li, Q. Li, K. Zhao, and J. Huang, "Eeg-based volitional control of prosthetic legs for walking in different terrains," *IEEE Transactions on Automation Science and Engineering*, vol. 18, no. 2, pp. 530–540, 2019.

[22] J. Andreu-Perez, F. Cao, H. Hagras, and G.-Z. Yang, "A self-adaptive online brain–machine interface of a humanoid robot through a general type-2 fuzzy inference system," *IEEE Transactions on Fuzzy Systems*, vol. 26, no. 1, pp. 101–116, 2016.

[23] L. Tonin, F. C. Bauer, and J. d. R. Millán, "The role of the control framework for continuous teleoperation of a brain–machine interface-driven mobile robot," *IEEE Transactions on Robotics*, vol. 36, no. 1, pp. 78–91, 2019.

[24] D. Liu, W. Chen, Z. Pei, and J. Wang, "A brain-controlled lower-limb exoskeleton for human gait training," *Review of Scientific Instruments*, vol. 88, no. 10, 2017.

[25] J. R. Millan and J. Mouriño, "Asynchronous bci and local neural classifiers: an overview of the adaptive brain interface project," *IEEE transactions on neural systems and rehabilitation engineering*, vol. 11, no. 2, pp. 159–161, 2003.

[26] L. Junwei, S. Ramkumar, G. Emayavaramban, M. Thilagaraj, V. Muneeswaran, M. P. Rajasekaran, V. Venkataraman, A. F. Hussein *et al.*, "Brain computer interface for neurodegenerative person using electroencephalogram," *IEEE Access*, vol. 7, pp. 2439–2452, 2018.

[27] T. Li, J. Hong, J. Zhang, and F. Guo, "Brain–machine interface control of a manipulator using small-world neural network and shared control strategy," *Journal of neuroscience methods*, vol. 224, pp. 26–38, 2014.

[28] Z. Tang, S. Sun, S. Zhang, Y. Chen, C. Li, and S. Chen, "A brain-machine interface based on erd/ers for an upper-limb exoskeleton control," *Sensors*, vol. 16, no. 12, p. 2050, 2016.

[29] G. Kucukyildiz, H. Ocak, S. Karakaya, and O. Sayli, "Design and implementation of a multi sensor based brain computer interface for a robotic wheelchair," *Journal of Intelligent & Robotic Systems*, vol. 87, pp. 247–263, 2017.

[30] F. S. Racz, R. Fakhreddine, S. Kumar, and J. Del R. Millan, "Riemannian geometry-based detection of slow cortical potentials during movement preparation," in *2023 11th International IEEE/EMBS Conference on Neural Engineering (NER)*, 2023, pp. 1–5.

[31] A. Barachant, S. Bonnet, M. Congedo, and C. Jutten, "Multiclass brain–computer interface classification by riemannian geometry," *IEEE Transactions on Biomedical Engineering*, vol. 59, pp. 920–928, 2012. [Online]. Available: https://api.semanticscholar.org/CorpusID:423006

[32] S. Calinon, "Gaussians on riemannian manifolds: Applications for robot learning and adaptive control," *IEEE Robotics & Automation Magazine*, vol. 27, pp. 33–45, 2019. [Online]. Available: https://api.semanticscholar.org/CorpusID:216322247

[33] G. Schalk, D. McFarland, T. Hinterberger, N. Birbaumer, and J. Wolpaw, "Bci2000: a general-purpose brain-computer interface (bci) system," *IEEE Transactions on Biomedical Engineering*, vol. 51, no. 6, pp. 1034–1043, 2004.

[34] L. McInnes and J. Healy, "Umap: Uniform manifold approximation and projection for dimension reduction," *ArXiv*, vol. abs/1802.03426, 2018. [Online]. Available: https://api.semanticscholar.org/CorpusID:3641284

[35] J. A. Pineda, B. Z. Allison, and A. Vankov, "The effects of self-movement, observation, and imagination on/spl mu/rhythms and readiness potentials (rp's): toward a brain-computer interface (bci)," *IEEE Transactions on Rehabilitation Engineering*, vol. 8, no. 2, pp. 219–222, 2000.

[36] W. Wen, R. Minohara, S. Hamasaki, T. Maeda, Q. An, Y. Tamura, H. Yamakawa, A. Yamashita, and H. Asama, "The readiness potential reflects the reliability of action consequence," *Scientific Reports*, vol. 8, 2018. [Online]. Available: https://api.semanticscholar.org/CorpusID:51940807